Environmental Science and Ecotechnology 22 (2024) 100480

Contents lists available at ScienceDirect

Environmental Science and Ecotechnology

journal homepage: www.journals.elsevier.com/environmental-science-and-ecotechnology/

Review

Mass transfer in heterogeneous biofilms: Key issues in biofilm reactors and AI-driven performance prediction

Huize Chen [a, b], Ao Xia [a, b, *], Huchao Yan [a, b], Yun Huang [a, b], Xianqing Zhu [a, b], Xun Zhu [a, b], Qiang Liao [a, b]

[a] Key Laboratory of Low-grade Energy Utilization Technologies and Systems, Chongqing University, Ministry of Education, Chongqing, 400044, China
[b] Institute of Engineering Thermophysics, School of Energy and Power Engineering, Chongqing University, Chongqing, 400044, China

ARTICLE INFO

Article history:
Received 25 November 2023
Received in revised form
23 August 2024
Accepted 26 August 2024

Keywords:
Biofilm
Reactor
Heterogeneous structure
Mass transfer
Artificial intelligence

ABSTRACT

Biofilm reactors, known for utilizing biofilm formation for cell immobilization, offer enhanced biomass concentration and operational stability over traditional planktonic systems. However, the dense nature of biofilms poses challenges for substrate accessibility to cells and the efficient release of products, making mass transfer efficiency a critical issue in these systems. Recent advancements have unveiled the intricate, heterogeneous architecture of biofilms, contradicting the earlier view of them as uniform, porous structures with consistent mass transfer properties. In this review, we explore six biofilm reactor configurations and their potential combinations, emphasizing how the spatial arrangement of biofilms within reactors influences mass transfer efficiency and overall reactor performance. Furthermore, we discuss how to apply artificial intelligence in processing biofilm measurement data and predicting reactor performance. This review highlights the role of biofilm reactors in environmental and energy sectors, paving the way for future innovations in biofilm-based technologies and their broader applications.

1. Introduction

1.1. Bioenergy production and microbial conversion

In recent decades, the global energy demand has surged, posing significant challenges in production and utilization. By 2030, it is expected to rise by 39% due to population growth, industrialization, and urbanization [1,2]. About 80% of the world's energy needs are met by fossil fuels; however, their finite reserves and geopolitical instability are problematic, leading to increasing interest in renewable energy [3]. Biofuels are an example of a renewable energy source and can be produced using various feedstocks, such as agricultural residues, forestry waste, municipal solid waste, and aquatic biomass. About 4.6 gigatonnes of wood-derived biomass is produced annually, and much of this is wasted [4]. Agricultural residues have an energy potential of 15–70 EJ per year [5], and the volume of municipal solid waste is projected to rise from 2 billion tonnes to 3.4 billion tonnes by 2050 [6]. Utilizing these waste streams to produce biofuels can mitigate environmental issues and convert waste into valuable energy [7].

There is growing interest in transforming organic waste into bioenergy and biofuels using microbes due to the sustainability and efficiency of the process [8]. Microbial conversion of waste is environmentally friendly and occurs under normal conditions without the need for high temperatures or pressures. Given that microbes target specific waste components, there is no need for pre-separation and purification steps, which improves efficiency. Microbe-mediated energy production can also be performed locally, reducing transportation costs and logistics.

Bioreactors are essential in microbe-mediated energy production to create an optimal environment for microbial activity. However, challenges are associated with using traditional bioreactors containing suspended cells. For example, it is difficult to maintain a high biomass density using such reactors because cells are lost in the effluent, limiting their capacity to handle concentrated feedstocks [9]. The risk of biomass loss and instability in the microbial community structure also exists [10]. To solve these

* Corresponding author. Key Laboratory of Low-grade Energy Utilization Technologies and Systems, Chongqing University, Ministry of Education, Chongqing, 400044, China.
E-mail address: aoxia@cqu.edu.cn (A. Xia).

https://doi.org/10.1016/j.ese.2024.100480

List of abbreviations

EPS	Extracellular Polymeric Substances
AI	Artificial Intelligence
eDNA	Extracellular Deoxyribonucleic Acid
SEM	Scanning Electron Microscopy
ESEM	Environmental Scanning Electron Microscopy
VP-SEM	Variable Pressure Scanning Electron Microscopy
AFM	Atomic Force Microscope
CLSM	Confocal Laser Scanning Microscopic
OCT	Optical Coherence Tomography
RGB	Red-green-blue
STR	Stirred-tank Reactor
FBBR	Fixed-bed Biofilm Reactor
TBR	Trickle-bed Bioreactor
MBBR	Moving Bed Biofilm Reactor
RDBR	Rotating Disc Biofilm Reactor
MBfR	Membrane Biofilm Reactor
BES	Bioelectrochemical System
EET	Extracellular Electron Transfer
DET	Extracellular Direct Electron Transfer
MET	Mediated Eelectron Transfer
MFC	Microbial Fuel Cell
DL	Deep Learning
ANN	Artificial Neural Networks
COD	Chemical Oxygen Demand
HRT	Hydraulic Retention Time
TN	Total Nitrogen
TP	Total Phosphorus
RMSE	Root Mean Square Error
SBBR-VFCW	Sequencing Batch Biofilm Reactor Combined with a Vertical Flow Constructed Wetland
MRBC	Membrane Rotating Biological Contactors
RSM	Response Surface Methodology
PDMS	Polydimethylsiloxane
ANN	Artificial Neural Networks

problems, a new generation of bioreactors has been developed, and microbial cells are immobilized to retain cells in the bioreactor during its continuous operation.

1.2. Biofilms as cell immobilization tools

Cell immobilization encompasses both active and passive methods. Active immobilization can involve using external agents to cross-link cells, attaching cells onto substrates via covalent bonds, or the entrapment of cells within porous matrices [11]. Conversely, passive immobilization relies on the natural adhesive properties of cells to form robust biofilms on various substrates, such as plastic [12], ceramic [13], biochar [14], glass [15], and loofah sponge [16]. Most biofilm reactors discussed in this article utilize passive methods for cell immobilization. It is also worth noting that microorganisms can attach to suspended particles in the reactor to form biomass granules and develop into biofilms [17]. However, since these solid particles are not intentionally introduced and their surface characteristics are not directionally regulated, they are not within the scope of this discussion.

Biofilm-based systems have numerous benefits, including improved environmental tolerance, highly active biomass, extended biomass retention, low space requirements, operational flexibility, and diminished hydraulic retention times [18–20]. Additionally, these systems allow for enhanced control over the microbial community structure and kinetic rates [21].

Introducing conductive materials as biofilm carriers has been a novel approach to improve anaerobic digestion performance. Specific conductive supports, such as magnetite [22], active carbon [22–24], and graphite [25], have been selected for their capacity to facilitate interspecies electron transfer. This property reduces the reliance on hydrogen as an electron shuttle and thus significantly augments the efficiency of biogas production within reactors [26,27].

Biofilm development is crucial for setting up a biofilm reactor. Biofilm formation is initiated when microorganisms shift from a free-floating state to an attached state on a surface, influenced by cell density, nutrients, and stress [28]. The process begins with reversible attachment to a surface and progresses to irreversible adhesion. The attached cells then grow and form mature biofilms [29]. Growth increases the thickness of the biofilm; however, the thickness is limited by nutrient depletion and waste accumulation, which lead to cell detachment and dispersal. Thus, a balance exists between cell detachment and adhesion. Within biofilms, cells are embedded in a self-produced extracellular polymeric substance (EPS) matrix, which includes polysaccharides, proteins, lipids, and extracellular deoxyribonucleic acid (DNA) [30,31]. The EPS matrix supports the biofilm's structure, protects against shear forces, retains enzymes, resists antimicrobials, and creates a stable microenvironment [32–34].

1.3. The heterogeneous structure of biofilms

Upon the maturation of a biofilm on a carrier, mass transfer processes within the biofilm emerge as critical effects that govern the reaction kinetics. Although an increase in the biofilm thickness can yield higher biomass, an increase in the mass transfer resistance induced by the over-accumulation of biomass may lead to cells located at the bottom of the biofilm facing a nutrient deficiency. This can result in an accumulation of dead cells, potentially threatening the mechanical stability of the entire biofilm and, consequently, the performance at the reactor level [35].

Early one-dimensional (1-D) biofilm models focus on the gradient perpendicular to the biofilm–liquid interface and treat the biofilm as a uniformly porous medium. Later, two-dimensional and three-dimensional (3-D) models consider the distribution of biomass and solute gradients and thus provide a more accurate depiction of new biomass distribution [36]. However, these models still have difficulty describing specific internal biofilm structures. Additionally, traditional models consider mass transfer from the bulk liquid to the biofilm as diffusion-dominated, neglecting the flow within the biofilm's heterogeneous channel structures [36,37]. The heterogeneous model is increasingly being scrutinized due to the emergence of new information about the inherent spatial structure of biofilms revealed by the use of advanced imaging techniques [38]. Remarkably, the delicate structure of biofilms has been found to facilitate/impede mass transfer [39,40]. Moreover, differences in the biofilm microenvironment may result in resident cells having different growth and metabolic activities and/or in the coupling of spatial and community structures. Acknowledging the synergistic effects within and between these heterogeneous structures and their mass transfer processes is essential for accurately assessing and improving the operational efficiency of biofilm reactors.

The heterogeneous structure of biofilms does not simply imply a spatially uneven distribution of biomass but rather indicates the existence of unique biofilm architectural elements (e.g., wrinkles, channels, barriers, stratifications) that combine to critically modulate solute transport, microbial activity, and inter-community interactions and thus have substantial repercussions for the conversion efficiency of biofilm reactors. However, there remains a discernible deficit in the literature regarding the intricacies of biofilm architecture and its effects on mass transfer processes despite its importance to the development of biofilm reactors. On a positive note, advanced measurement techniques have recently been employed to explore the microstructure of biofilms at high resolution, and current mathematical models can simulate the generation of some heterogeneous structures at the single-cell scale [41]. However, building on this to achieve mass transfer and reaction modeling for predicting reactor performance presents a significant challenge in terms of computational cost [42].

This review endeavors to bridge the abovementioned knowledge gaps, focusing on mass transfer in various biofilms and highlighting the effect of the heterogeneous structure of biofilms on mass transfer efficiency. The progress in using artificial intelligence (AI) algorithms for processing biofilm measurement data and for modeling and performance prediction of biofilm reactors is also discussed.

2. Biofilm architecture and mass transfer

In early research, biofilm models were simplistic, zero-dimensional (0-D) constructs that treated the biofilm as a homogeneous part of the biomass within biofilm reactors, ignoring the intricacies of mass transfer and biological reactions [36]. To address the spatial distribution of the characteristics of biofilms, 1-D biofilm models were introduced, which take into account the axial variation across the biofilm's thickness (e.g., in the porosity and EPS concentration) [43]. These models conceptualize the biofilm as a porous medium in which solute diffusion is akin to diffusion in water but adjusted using a tortuosity factor [44,45]. This factor, which reflects the biofilm's porosity and is influenced by the biomass density or the EPS matrix, provides a convenient understanding of solute movement within the biofilm structure. However, it was observed that the effective biomass diffusion coefficients exhibit a broad distribution due to the internal heterogeneous structure of biofilms [44,46]. Consequently, relying solely on mean diffusion coefficients may not adequately represent the mass transport processes in biofilms. Moreover, under certain flow conditions, convective mass transfer can lead to a higher mass transfer efficiency in the biofilm than a purely diffusion-driven process [47]. In some biofilm discrete models, the permeability of the cell membrane is simulated to indirectly describe the material exchange process between the inside and outside of the cells, eliminating the need to directly specify the diffusion coefficient [48].

2.1. The biofilm structure can hinder mass transfer

The movement of soluble constituents within biofilm structures is significantly impeded by the biofilm matrix, which results in a marked decrease in diffusivity compared to that in pure water. The degree of reduction can vary widely, with factors (relative effective diffusivity) ranging from 0.2 to around 0.8 [44–46]. This variability can be attributed to the intricate and diverse architecture of biofilm matrices. Notably, when considering specific structural features within biofilms, the transport of solutes can be markedly restricted at a microscale level (Supplementary Material Table S1). For example, *Bacillus subtilis* biofilms grown on a biomineralization medium containing calcium acetate were shown to form a dense and structured calcium carbonate lamina on their surface, which hindered the diffusion of water and small molecules (Fig. 1a) [49]. You et al. [50] found that exposure to ceria nanoparticles could enhance EPS production of biofilms, elevate the local mass transfer resistance, and prevent continued damage by heavy metal ions. Furthermore, Dunsing et al. [39] showed that the EPS matrix of *Pantoea stewartia* biofilms could function selectively as a reactive molecular sieve, modulating the transport of molecules and pathogens according to their size and surface characteristics rather than acting as a fully inert barrier.

While local barrier structures are widely present within various biofilms and play a considerable role in protecting the internal cells from the threats posed by antibiotics, oxygen [51] (Fig. 1b), and phages [52], they cannot be represented by conventional models. Evidence suggests that anaerobic microorganisms in biofilms are protected by the formation of mid-gaps and upper layers of aerobic cells that actively utilize oxygen, which could cause a sharp drop in the oxygen concentration between the top and the bottom of a biofilm (Fig. 1b) [51,53]. The oxygen concentration gradient has been shown to align with the abundance gradient of certain species within mature biofilms [53]. Additionally, when there is an oxygen concentration gradient and the hydraulic shear stress experienced by a biofilm is controlled, it is possible to establish aerobic and anaerobic stratification and control the compactness or looseness of its cellular layers [54]. Similarly, the EPS matrix has been observed to possess a stratified structure (an outer layer rich in active biomass and polysaccharides and a basal layer rich in dissolved products and proteins) and porosity (a highly porous outer layer and a less porous basal layer). These differences are primarily attributed to the limitations in nutrient mass transfer and cell decay [55].

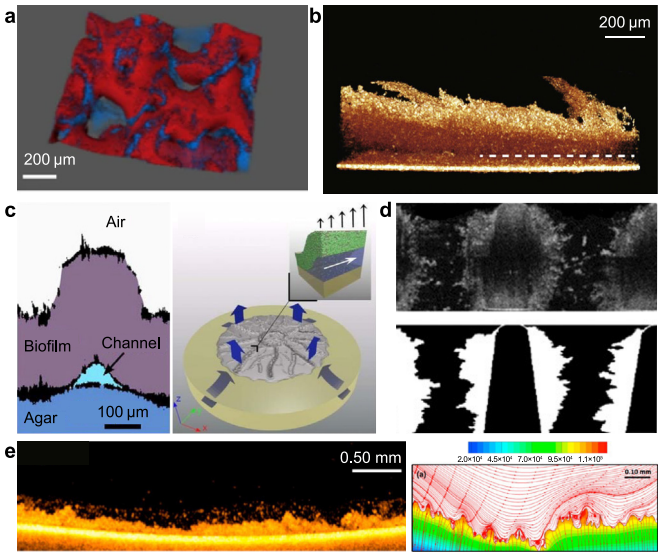

Fig. 1. The heterogeneous architecture in biofilms. **a**, 3-D reconstruction of topography of biofilm surface, red indicates the densest mineral. Reprint from Ref. [49]. Copyright 2018. Springer Nature. **b**, The sparse gap between the dense inner layer and the dense outer layer of biofilms. Reprint from Ref. [51]. Copyright 2019. Cell Press. **c**, Side view of the channel in biofilm (left); Illustration of evaporation from the surface of the film (blue arrows) that drives liquid flow throughout the biofilm (right). Reprint from Ref. [40]. Copyright 2013. National Academy of Sciences. **d**, Cross-sectional OCT images of biofilm developed on the carrier (top); Biofilm profile obtained by threshold method (bottom). Reprint from Ref. [72]. Copyright 2015. John Wiley & Sons, Inc. **e**, OCT images of biofilm developed on the substrate (left); Importing OCT image information into Computational Fluid Dynamics to obtain the absolute pressure contour and stream trace plots (right). Reprint from Ref. [73]. Copyright 2017. Elsevier.

Exposure to predators induces EPS production, and while this mechanism can protect cells within the biofilm from toxic agents, the resultant increases in the thickness and biomass density concurrently diminish the mass transfer efficiency. The subsequent lack of nutrient delivery to cells deep within the biofilm can lead to cell death and the accumulation of dead cells, which may decrease the performance of the entire biofilm [56–58]. To counteract this issue, quorum-quenching bacteria have been introduced to regulate the thickness of biofilms and preserve their efficient mass transfer; this approach has been shown to disrupt bacterial communication and significantly decrease EPS production, resulting in relatively thin and dense biofilms [59,60]. Introducing predators into inactive growth regions of biofilms can enlarge cavities and induce biofilm detachment, and this strategy can be applied to improve mass transfer issues in overly thick biofilms [61]. Introducing an appropriate heavy metal ion concentration can stimulate EPS secretion, especially the secretion of extracellular proteins, to maintain the effective capacity of substrate uptake while protecting cells [62]. In addition, incorporating tourmaline into the biofilm formation process has enhanced EPS secretion. The electric dipole effect encourages bacteria to synthesize more EPS, which not only aids in self-protection under harsh conditions but also improves the nitrogen removal efficiency of the reactor [63].

The heterogeneous structure of biofilms affects the transfer of substrates and metabolites. Dense biofilms increase the concentration of acidic by-products and the difficulty of their dispersion, which means that the pH is generally lower in microcolonies than in the bulk phase [64]. Dhar et al. [65] reported pH differences of 0.3–0.5 throughout the depth of biofilms (approximately 100 μm). Such pH gradients significantly affect the distribution of active microorganisms in biofilms and may affect a biofilm's electrical conductivity. In other cases, a pH gradient was consistent with the cell density distribution and structure of the EPS matrix [66], emphasizing the association between the biofilm structure and the mass transfer of protons. These findings indicate that immobilizing acid-producing microorganisms may lead to reactor-scale failure due to localized acidification within biofilms.

2.2. The biofilm structure can facilitate mass transfer

Some biofilm structural components enhance the mass transfer (Supplementary Material Table S1). For example, voids and flow channels can significantly augment nutrient flux, as was shown using a *B. subtilis* biofilm grown on the surface of agar that developed an intricate network of channels that promoted radial liquid flow within the biofilm (Fig. 1c) [40]. The formation of such channels has been attributed to mechanical instability between the biofilm and its substrate [67].

Electron transfer is notably influenced by the biofilm structure. In electrochemically active biofilms, cytochromes, conductive filaments, e-pilis, and redox shuttles are distributed heterogeneously, extending from the electrode surface and facilitating conductivity throughout the biofilm [68]. Notably, producing these extracellular electron mediators depends on establishing an optimal electrode potential. In instances of high potential, *Geobacter soli* biofilms have been observed to increase the production of electrically nonconductive extracellular polysaccharides, particularly in their inner layers. This could be a protective mechanism whereby physical barriers are formed to shield cells near electrodes from the heightened stress caused by the electrodes [69]. Biofilms of *Geobacter sulfurreducens* lacking certain multiheme cytochromes have been observed to form denser structures at the bottom, potentially enhancing the efficiency of electron transfer to electrodes [70]. Research has demonstrated that employing genetic engineering and introducing nickel ions induces the pilin proteins of *G. sulfurreducens* to coil, which results in a highly organized structure that enhances the efficiency of electron transfer within the biofilm, leading to more uniform bacterial activity within the biofilm [71].

In addition to the inner biofilm structure, the morphology of the biofilm surface — the essential interface between the biofilm and bulk phase — significantly affects the mass transfer process. The biofilm surface is usually rough, and when compared with smooth surfaces, rough biofilm surfaces are more conducive to nutrient transfer (Fig. 1d) [72]. The peak and cavity microstructures on the biofilm surface enhance the overall permeate flux by forming entrapped separation vortices (Fig. 1e) [73]. The heterogeneity of the biofilm surface can also lead to an increase in local shear stress, which can be up to three times the average wall shear stress, which may shape the biofilm's surface structure [74].

2.3. Mechanical stability of biofilms

The structure of a biofilm significantly impacts not only its mass transfer process but also its mechanical stability, which is vital for the biofilm's existence, particularly under conditions of non-negligible hydraulic shear [75]. The EPS matrix [76], appendages of cells (fimbria [77] and flagella [78]), and arrangement of the constituent cells [79] contribute to the biofilm structure, providing mechanical stability and scaffolds for building microconsortia. The mechanical robustness of biofilms is largely attributed to the EPS matrix, which provides indispensable cohesiveness, and the cohesive strength of biofilms has been recorded as 6.0–7.7 N m^{-2} [80,81]. The latest component analysis of a *B. subtilis* EPS matrix indicated that 10% of the biofilm consists of rigid regions, which provide mechanical stability and form a water barrier, and 90% of mobile regions, which allow nutrient circulation and impart structural flexibility [82]. The mechanical properties are similar to those of hydrogel, with variable viscoelasticity observed, depending on the strain, which affects the deformation and granulation of the biofilm under hydraulic shear [83]. In some biofilm reactors, there is an issue with the over-accumulation of biofilms, which can lead to the formation of biomass clots that clog the fluid and reduce the efficiency of mass transfer in the biofilms. Regulating the hydraulic shear stress to obtain biofilms with near-constant thickness and mass transfer rates is a solution. However, the heterogeneity of biofilm viscoelasticity makes the shedding of excess biomass difficult to predict. Such heterogeneous physical properties are derived from the heterogeneous distribution of EPS. Both experimental and simulation results have revealed that the viscoelasticity of biofilms aligns with the depth of the biofilm layer [52,84]. Even in the same layer, heterogeneous viscoelastic properties have been observed [85].

3. Advanced measurement technologies for determining the biofilm architecture and microenvironment

3.1. Techniques for biofilm measurement

Conventional scanning electron microscopy (SEM) is prevalent, particularly for examining biofilm surface and cross-sectional structures [27] (Table 1). However, this method requires dehydration and coating processes, which might cause the EPS matrix to collapse and overall biofilm shrinkage. Alternatives to conventional SEM for the analysis of biofilm architecture include environmental SEM (ESEM) and cryo-SEM. ESEM, also called variable pressure SEM, allows unpretreated biofilm samples to be directly placed in the microscope chamber whose pressure values are near the environmental value [86]. Biofilms in their natural state can be visualized, and dehydration artifacts and mass loss can be avoided

Table 1
Techniques for measuring the heterogeneity of biofilms.

Heterogeneity	Technique	Application	Advantage	Limitation	Remark	Reference
Architecture	SEM	Provides information about the surface/section structure	•Higher resolution •Qualitatively supportive •Wide ranges of magnification	•Sample preparation process destroy the structure of samples or cause artifacts	•Biofilm on the electrode surface •Thickness measurement through cross-sectional analysis	[27]
	Cryo-SEM	Provides detailed visualization of ultrastructures	•Detailed visualization of biofilm ultrastructure	•Expensive and specialized equipment •Sample melting and cracking	•*Pseudomonas aeruginosa* biofilm •The connections between cells were captured	[89]
	ESEM	Provides information about the surface structure	•Retains natural state of biofilms without pretreatment	•Relative low resolution •Sample damage (the absence of metal coating)	•*Streptococcus mutans* biofilm •The EPS structure was well-preserved and imaged	[86]
	CLSM	Reveals biofilm spatial structure and functions	•Compatibility with various fluorescent probes •Reconstruction of 3-D structures of a sample	•Local properties of biofilms are disturbed by fluorescent probes •Highly dependent on the applied fluorescent stains •Natural auto-fluorescence interference	•CLSM measure the distribution of solutes •CLSM measure the structure of biofilms	[96]
	OCT	Provides 3D spatial structure data of biofilms	•No pretreatment of samples required •*In-situ* and non-invasive	•Signal may be disturbed by interference	•The deformed biofilms under flow shear were measured	[104,109]
	AFM	Measures the adhesion forces and topography of biofilms	•Minimizes the need for pretreatment •Quantifiable	•Inability to obtain a large area information •Measurement results depend on the shape and size of the tip	•*Bacillus subtilis* biofilm •The interaction forces between cells and the substrate were measured	[90]
	Particle tracking	Measures the viscoelasticity properties of biofilms	•Non-destructive and real-time detection	•Surface properties of the probes may cause interference	•Diffusion and transport characteristics were analyzed	[95]
Microenvironment	Microelectrodes	Measure the concentrations of dissolved compounds in biofilms at micrometer scale	•Easy installation of equipment	•Resolution dependent on the tip size •Insertion of the tip may damage the original structure of the sample	•*Escherichia coli* biofilm •The pH distribution was measured	[112]
	Nanosensor	Measure the concentrations of dissolved compounds in biofilms at nanometer scale	•Provides high-resolution concentration information in 3-D space	•Needs to be customized for specific experiments	•*Pseudomonas fluorescens* biofilm •*Pseudomonas aeruginosa* biofilm •The distributions of pH, ions, and oxygen were measured	[66,113,114,116]

[87]. Aldehyde fixatives that specifically bind to lipids can be used to preserve the detailed features of biofilms. Heavy metal staining can also enhance the contrast and resolution in ESEM [88]. However, the sample damage caused by the focused electron beam and the relatively low resolution are still problems faced in ESEM. In contrast, cryo-SEM involves performing a fast cryo-fixation pretreatment to fracture biofilms and expose their inner structure. This method can allow a detailed visualization of the relationships between the biofilm's cells and EPS matrix ultrastructure [89]. However, high instrumental and administrative demands limit cryo-SEM application in biofilm research. Moreover, like ESEM, cryo-SEM carries the risk of sample damage due to using a focused electron beam.

Atomic force microscopy (AFM) is a versatile tool in biofilm research, offering *in situ* imaging of biofilm topography and insights into biofilm cohesion [90] (Table 1). The development of advanced algorithms has created the opportunity to use AFM to analyze the elasticity of the EPS matrix in biofilms at the nanoscale [91]. One major limitation of this technique is the restricted area over which it can gather information. Beyond topographical imaging, AFM has been integrated with microrheology to study the heterogeneous structural evolution of growing biofilms [92]. Particle tracking is another useful method for measuring the viscoelastic properties of biofilms [93]. However, it is important to note that the surface properties of the probes used in particle tracking can significantly influence the results. This fact imposes stringent requirements on probe design to ensure accurate measurements [94,95].

Confocal laser scanning microscopy (CLSM) has become a pivotal tool in biofilm research [96] (Table 1). Using appropriate staining techniques, CLSM can be used to concurrently reveal the spatial distribution of cells, polysaccharides, proteins, extracellular DNA (eDNA), and lipids within biofilms [97–100]. Ye et al. [58] went a step further and quantitatively compared these components using a methodology based on the fluorescence intensity of the molecules. The quantification of the live cell-to-dead cell ratio in biofilms is now a standard approach for assessing biofilm activity, which is facilitated by using staining methods [101]. Microscale information collected using CLSM can also be integrated with that resulting from microrheology to explore the mechanical properties of biofilms [102]. However, the efficacy of CLSM in visualizing biofilm structures is heavily contingent upon the choice of fluorescent stains and their capacity to interact with biofilms. For example, labeling all EPS matrix components is challenging since the EPS matrix in biofilms is complex and not a well-defined polymer [31,103]. Additionally, fluorescent probes may perturb local biofilm properties, and the issue of natural autofluorescence is an ongoing challenge.

Optical coherence tomography (OCT) is now extensively utilized to detect biofilms at lower micrometer levels [104] (Table 1). It is based on low-coherence interferometry and typically employs near-infrared light, which enables the acquisition of information on the 3-D structure of biofilms. This *in situ*, non-invasive technique negates the need for sample pretreatment and avoids sample damage during detection [105–107]. It also allows real-time monitoring of biofilm development. For instance, Fortunato et al. [73] used OCT to track biofilm formation for up to 43 consecutive days and collected *in situ* documentation of the entire biofilm formation process.

The compactness and portability of OCT devices enhance the practicality of incorporating OCT into experimental systems. Gierl et al. [108] demonstrated this by using an OCT device to develop a platform for automated biofilm growth monitoring, contributing insights into addressing reproducibility issues in biofilm studies. The non-destructive, online measurement capabilities of OCT facilitate the imaging of biofilms under dynamic conditions, allowing for real-time, time-lapse analysis of biofilm behavior [109]. As a tool for characterizing mesoscale biofilm structures, OCT effectively bridges the gap between micro- and macroscale analyses. It can also be used to perform quantitative analyses through calibration, such as biofilm density [110] and total N content [111] analyses. However, a significant challenge persists in applying OCT in biofilm research: signal interference due to the technique's reliance on recording reflected signals.

Microelectrodes have been the predominant tool for measuring dissolved solute concentrations in biofilms for several decades (Table 1). However, the resolution achievable with microelectrodes is largely contingent on the tip's size, and their insertion can potentially disrupt the native structure of the sample [112]. Furthermore, microelectrodes are limited to providing 1-D data along the depth of the biofilm. The advent of advanced measurement technologies has enabled the acquisition of 3-D, high-resolution microenvironmental data. In recent developments, nanosensors have been deployed to map the distribution of various solutes within biofilms. These nanosensors can be embedded within biofilms, ranging from 50 to 200 nm in diameter (Table 1). They respond to fluctuations in analyte concentrations by altering their optical properties, thus offering a means to monitor changes *in situ* [113]. For example, luminescent nanosensors have been utilized to generate 3-D oxygen profiles within *Pseudomonas aeruginosa* biofilms [114], while fluorescent mesoporous silica nanosensors have provided detailed 3-D pH mapping in *Pseudomonas fluorescens* biofilms [66]. These nanosensors are not limited to providing static measurements; they can also be used to dynamically track pH gradients present during biofilm formation with high spatial and temporal resolution [115,116]. It will be crucial to characterize the interactions between nanosensors, cells, and other biofilm components to ensure that introducing nanoparticles does not result in interference. As the repertoire of nanosensors expands, this technique holds promise as a measurement method that could gain wider adoption in research.

3.2. Advances in artificial intelligence for biofilm measurement and analysis

Many traditional biofilm measurement methods involve time-consuming sampling and pretreatment processes; thus, laboratories commonly use less reliable procedures to analyze biofilms. Recently, there has been a notable shift toward developing AI methods for rapidly acquiring critical biofilm characteristic parameters. A parameter that is essential in evaluating the start-up performance of biofilm reactors is the coverage area of biofilms on support materials. Microscopic techniques, such as CLSM and SEM, have been employed to assess biofilm colonization, and they are often used to obtain quantitative data on the biofilm area, volume, and thickness through segmentation and thresholding approaches. However, manual image processing can introduce significant errors due to subjective biases [117]. AI-based methods are emerging as a more precise means to quantify biofilm colonization, and image analysis techniques have been developed to accurately segment biofilms from backgrounds [118].

Microscopy can provide detailed images of biofilm surface structures that can be used to estimate geometric characteristics, determine the growth stage of the biofilm [119], and even characterize the bacterial composition [120], offering advances over traditional manual methods. Integrating AI methods has led to the development of more efficient visible light image-based analysis techniques for biofilm studies. These methods circumvent the complexities of sample preparation and facilitate real-time detection. Specifically, red-green-blue analysis has been used to assess the thickness of microalgal biofilms and has shown satisfactory

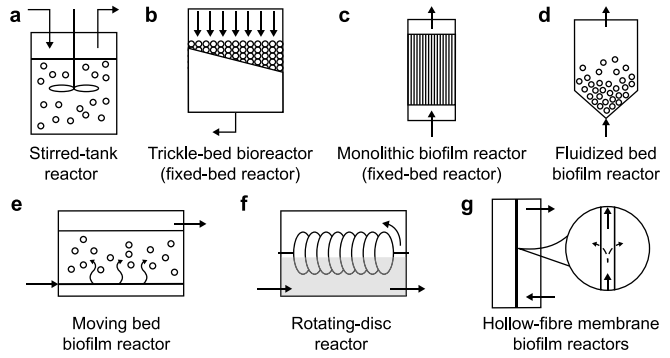

Fig. 2. Different types of biofilm reactors. a, Stirred-tank reactor. **b**, Trickle-bed bioreactor. **c**, Monolithic biofilm reactor. **d**, Fluidized bed biofilm reactor. **e**, Moving bed biofilm reactor. **f**, Rotating disc biofilm reactor. **g**, Membrane biofilm reactor.

accuracy [121]. In the future, artificial neural networks (ANNs) may inspire reconstructing the 3-D structure of biofilms from optical information. However, a notable limitation of current research is that it predominantly focuses on single-species biofilms. Hence, there is an urgent need to refine the existing AI-driven methods to have broader applications, particularly in analyzing multi-species biofilms, as found in biofilm reactors. Moreover, biofilms with gas bubbles or precipitates introduce an additional level of complexity, and addressing this gap is essential for advancing the field and enhancing the utility of AI in biofilm research.

4. Mass transfer in biofilm reactors

4.1. Stirred-tank reactors

Stirred-tank reactors (STRs) are derived from the classical reactors used in chemical engineering, and support materials are added for biofilm formation (Fig. 2a). Benefiting from continuous mechanical stirring, STRs have excellent mixing performance. However, for syngas fermentation, STRs require a substantial amount of energy to disperse large volumes of gas into the liquid phase and ensure contact between low-solubility gases and suspended carriers (1000–10,000 W m^{-3}) (Fig. 3b) [122]. In addition, sensitive microorganisms may be damaged by high local energy dissipation rates near the agitators or bursting gas bubbles at the surface [123].

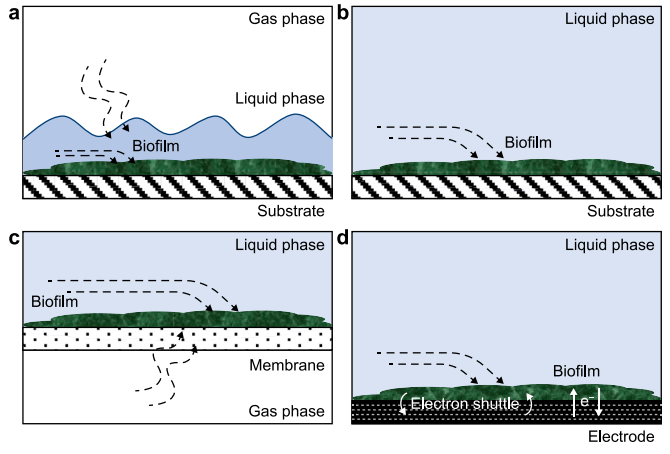

Fig. 3. Mass transfer pattern within biofilms. a, Biofilm coved with a thin liquid film. **b**, Biofilm submerged in liquid bulk phase. **c**, Biofilm attached on the porous membrane. **d**, Biofilm attached on the electrode. The dashed lines indicate the direction of mass transfer.

4.2. Fixed-bed biofilm reactors

Fixed-bed biofilm reactors (FBBRs, or packed-bed reactors) contain a fixed and dense biofilm support. With its large area of support providing highly efficient biomass–liquid contact and efficient biomass harvesting, the FBBR is arguably the most frequently used reactor for cultivating immobilized cells [124–126]. The trickle-bed bioreactor (TBR) is a commonly used type of FBBR (Fig. 2b). In TBRs, the liquid flows down through the packed material, which has a large surface area, and the gas phase moves either downward (co-current) or upward (countercurrent). As the liquid trickles down, forming a thin liquid film over the biofilm surface allows the efficient transfer of the gas phase, penetrating the biofilm (Fig. 3a) [127].

The use of a reactor containing wetted biocomposite porous paper as the biofilm support has been reported [122]. In this system, the liquid phase flows down the biocomposite as a very thin film generated at a low Reynolds number with countercurrent or co-current gas flow, and very high mass transfer rates are achieved. Another study highlighted the use of crushed clay as the biofilm carrier due to its large wetted carrier surface area and capacity to induce liquid turbulence [128]. The use of polyurethane foam as a biofilm carrier has also been investigated; it not only provides a larger gas-liquid contact area but also prolongs the residence time of bubbles in the packing layer, thereby enhancing the efficiency of biological conversion of hydrogen and carbon dioxide into methane [129]. Polyurethane foam has significant application potential, especially considering the low solubility of hydrogen [130].

Monolithic biofilm reactors contain a series of straight, parallel channels separated by thin and porous walls, and gas bubbles are forced through the channels (Fig. 2c) [131]. Employing such a design can reduce the frictional forces of the gas-liquid mixed flow and the thickness of the boundary layer between the gas and the biofilm cells. The thin layer of liquid at the biofilm surface demonstrates a plug flow pattern within the channels, which supports better mass transfer. The flow pattern, which dominates the mass transfer efficiency between the fluid and biofilm, depends on the fluid flow rate, channel geometry, and other factors (Fig. 3a and b) [132]. Additionally, liquid atomization has enhanced gas-to-liquid transfer in an FBBR and achieved greater productivity [133].

4.3. Fluidized-bed bioreactors

In fluidized-bed bioreactors, cells are immobilized onto solid particles, and high biomass concentrations (30–40 kg m^{-3}) have been reported (Fig. 2d) [134]. Fluidization of the biofilm particles is achieved by the upward flow of the liquid and/or gas phase, and the degree of mixing within these reactors is considered intermediate: between that of FBBRs and STRs [135]. The use of smaller particles than those in other attached-growth systems, such as moving bed biofilm reactors (MBBRs), results in much thicker biofilms and more biofilm surface being exposed to the water, allowing the treatment of feedstock that contains larger compounds and that is delivered at high concentrations [136]. The hydrodynamic system, which provides a good mixture in the fluidized bed, has sufficient gas-liquid contact, gas supply, and gas removal. The use of a reactor containing a fluidized bed, a photoreactor, and activated carbon fibers as the carrier has been reported, and this combination of components was found to increase the maximum hydrogen yield and production rate to 33.6% and 65.8%, respectively [137]. A fluidized-bed bioreactor has also been used to produce biohydrogen via dark fermentation; in this system, the up-flow

velocities were sufficient to extract the produced H_2 and avoid inhibition by its accumulation and partial pressure [138].

Moving bed biofilm reactors employ inert carriers (usually made of plastic) that are held in suspension throughout the reactor, and the turbulent energy is supplied by aeration, liquid recirculation, or mechanical mixing (Fig. 2e). Carriers typically make up 30–60% of the volume in such reactors [139]. MBBRs tend to utilize biofilms with very specific metabolic activities, and the conditions within reactor are developed to support the growth of such biofilms. Optimizing the growth of functionally active microbes leads to high volumetric productivity and increased process stability, resulting in a reactor with a compact structure. In addition, MBBRs are less prone to bed clogging, a common issue with other attached-growth bioreactor configurations, due to continuous mixing. The steady productivity of MBBRs is attracting increasing attention in biofuel production, particularly for the production of biohydrogen [140] and ethanol [141]. A recent study showed that an MBBR outperformed a suspended-culture reactor under high-pressure conditions, overcoming the primary bottleneck of gas transfer and demonstrating a 33% higher H_2 uptake and 48% higher acetic acid production rate [142]. The biofilms on the carriers were easy to collected to assess their thickness and morphology, and the biomass and biofilm characteristics were quantitatively analyzed; such analyses can be useful when troubleshooting reactor malfunctions and optimizing reactor performance [143].

4.4. Rotating disk biofilm reactors

Rotating disk biofilm reactors (RDBRs) use disks as the biofilm support. The disks are mounted on a rotary shaft. The biofilms on the disks are alternately exposed to the atmosphere and the liquid phase (Fig. 2f). When a biofilm on a disk enters the atmosphere from the liquid phase, the thin liquid film residual on the biofilm surface greatly reduces the mass transfer resistance of the gas phase. Interestingly, RDBRs have been used to simulate scenarios with special mass transfer conditions, such as marine strain biofilms under the effect of tides [144]. When the rotating disk is in contact with the gas phase, it is subjected to good light transmission conditions; therefore, RDBRs have been widely used to cultivate photosynthetic microorganisms [145].

There is growing interest in using RDBRs for syngas fermentation due to their good gas-phase mass transfer efficiency. The use of a rotating packed-bed reactor that combined FBBR and RDBR technology and contained biofilm carriers packed in a cage-like enclosure has been investigated [141]. The biofilms attached to the carriers were alternately in contact with the liquid and gas phases, and the thin liquid film on the biofilms decreased the transfer resistance for gas diffusion. This reactor achieved an ethanol productivity rate of 6.7 g L^{-1} d^{-1}, 3.3 times higher than that achieved using an STR.

4.5. Membrane biofilm reactors

Membrane biofilm reactors (MBfRs) are designed to achieve an independent supply of the gas and liquid phases. MBfRs employ a gas-permeable membrane that delivers gaseous substrates to the biofilm formed on the outer surface of the membrane when the biofilm is submerged in liquid (Fig. 2g). Unlike biofilms in other types of reactors, the biofilm in an MBfR mediates counter-gradient diffusion of electron donor and acceptor substrates, allowing efficient mass transfer (Fig. 3c) [146,147]. The gas-phase mass transfer process includes premixing of the gas before it enters the membrane, gas boundary layer transfer, transfer through the membrane, diffusion through and consumption within the biofilm, and boundary layer transport through the liquid phase. Controlling the aeration method can influence the width of the aerobic zone within the biofilm, thereby regulating the production/consumption mechanisms of nitrogen oxides [148].

The composition and structure of the membrane play important roles in the mass transfer process. Membranes with large pore sizes (0.01–1 mm) have been shown to provide insufficient operational transmembrane pressure, which can cause the membrane pores to fill with water, increase the mass transfer resistance or the formation of bubbles at the liquid side, and ultimately destroy biofilms [149]. Since polydimethylsiloxane (PDMS) can effectively isolate liquids while maintaining good gas permeability and has excellent biocompatibility and mechanical properties, it has received widespread attention as a membrane material. Additionally, modifying PDMS can optimize its selectivity and permeability for specific gas components [150].

The membrane used in reactors designed for industrial syngas fermentation should be arranged in a manner that efficiently and cost-effectively maximizes the interfacial area per volume unit. Regarding this aspect, hollow-fiber membrane biofilm reactors with low manufacturing costs have been found to outcompete other configurations. They are the most commonly used reactors for gas-liquid membrane contact applications [151,152]. The distinct layout of the hollow-fiber membrane in such reactors may cause different flow patterns and result in various mass transfer characteristics [152]. A dual-membrane aerated biofilm reactor has been developed to address the issue of significant differences in gas solubility in membrane biofilm reactors. This reactor simultaneously uses different hollow-fiber membranes tailored to various gases [153]. Adjusting the partial pressures of different gases is also a convenient way to achieve changes in the metabolic pathways of microorganisms within the biofilm [154].

4.6. Bioelectrochemical systems

Cells are immobilized (via a passive method) in bioelectrochemical systems (BESs), and BESs are considered a novel and promising platform for environmental remediation and syngas fermentation. They facilitate oxidation and reduction reactions in their anode and cathode chambers. Unlike in other types of biofilm reactors, in addition to solute transfer within biofilms, extracellular electron transfer occurs between the microbes and the electrode in BESs via extracellular direct electron transfer (DET) or mediated electron transfer (MET) (Fig. 3d). DET needs direct physical connections between the electron donor/acceptor microbes and the redox-active surface via electron mediators, such as cytochromes, multicopper proteins, and pilin proteins, and the diffusion of a soluble electron shuttle is unnecessary [155,156]. MET requires electron shuttles to transport the electrons.

BESs can be integrated with other biofilm reactors to enhance productivity. For instance, an electro-MBBR system has been developed in which the cathode and anode are positioned at the bottom of the reactor, facilitating *in situ* generation of H_2 microbubbles, and the MBBR component is placed above the electrodes, which increases the retention time of these bubbles within the reactor [157]. This setup reportedly achieved a maximum methane production rate of 1.42 L L^{-1} d^{-1} and a coulombic efficiency (electrons-to-methane) of up to 92.5%. Including electromethanogenesis has also broadened the adaptability of anaerobic digestion systems to extreme environments, such as those with high levels of toxicants [158], recalcitrant organics, and lower temperatures [159].

Various biofilm reactors that employ different biofilm support materials and configurations have been utilized in bioenergy production (Table 2). Contemporary advances in biofilm reactor technology have led to reactor systems that defy traditional

Table 2
Studies of bioenergy with biofilm technology.

Type	Application	Biofilm carrier	Remark	Reference
Fixed bed biofilm reactor	Microalgae biomass production	Fabric membrane	Microalgae productivity (10.14 g m^{-2} d^{-1})	[124]
Rotating bed biofilm reactor	Ethanol production	High-density polyethylene	Ethanol productivity (6.7 g L^{-1} d^{-1})	[141]
Membrane biofilm reactor	Ethanol production	Polypropylene	Batch-produced ethanol concentration (16.9 g L^{-1})	[154]
Membrane biofilm reactor	Ethanol production	Polypropylene	Ethanol productivity (3.44 g L^{-1} d^{-1})	[127]
Fixed bed biofilm reactor	Ethanol production	Ceramic	Ethanol (2.35 g L^{-1} day^{-1})	[131]
Fixed bed biofilm reactor	Hydrogen production	High-density polyethylene	Hydrogen productivity (252 mL L^{-1} h^{-1})	[125]
Moving bed biofilm reactor	Hydrogen production	High-density polyethylene	Outlet hydrogen concentration (19.5 mmol L^{-1})	[176]
Fixed bed biofilm reactor	Methane production	Polyurethane foam	Bioenergetic potential (6.3 kJ per g COD)	[129]
Microbial electrolysis cell	Methane production	Carbon brush and carbon cloth	Methane productivity (0.0681 m^3 m^{-3} d^{-1})	[156]
Fluidized-bed biofilm reactor	Methane production	Granular activated carbon and polyethylene	Methane yield (285 mL per g COD)	[24]
Membrane biofilm reactor	Methane production	Polypropylene	Maximum CH_4 content (97.6%)	[153]
Moving bed biofilm reactor	Methane production	High-density polyethylene	Methane productivity (1.42 L L^{-1} d^{-1})	[157]
Membrane biofilm reactor	Methane production	Polypropylene	Methane productivity (12 m^3 m^{-1} d^{-1})	[147]
Fixed bed biofilm reactor	Methane production	Polypropylene	Methane productivity (0.263 L per g COD), methane concentration (78%)	[126]

categorization and are often hybrids of multiple reactor types. For instance, materials typically used as moving carriers in MBBRs are now utilized as packed supports in RDBRs [141]. Similarly, mechanical stirring, a common feature in STRs, has been incorporated into MBBRs to enhance mixing [160]. Furthermore, electrodes have been integrated into MBBRs to generate hydrogen microbubbles, aiding mass transfer [157], and into anaerobic digestion systems to form electroactive biofilms and enrich electromethanogens [158,159]. In other examples of the merging of different technologies in single systems, optical hollow fibers have been added to a biofilm reactor to facilitate efficient light transport [161], and rotating disks have been added to a membrane biofilm reactor to explore the response of biofilms to hydraulic shear under aeration conditions [54].

Understanding the mass transfer characteristics of these diverse biofilm reactor configurations is crucial for developing novel reactors tailored to specific operational needs. However, traditional mathematical modeling of these complex systems poses significant challenges. The intricate solid/liquid/gas three-phase flow in various biofilm reactors necessitates extensive computational resources for computational fluid dynamics analysis. Furthermore, accurately predicting the dynamic interplay between the community structure and operating conditions within these reactors remains a formidable task. Consequently, conventional modeling methods that focus on physical and bioconversion processes struggle to balance computational efficiency with accurate predictions in the context of biofilm reactors. In response to these challenges, various AI-based algorithms have emerged as promising tools for modeling the complex processes inherent in biofilm reactors. These algorithms are also instrumental in processing biofilm structural data, offering a new frontier in optimizing and predicting biofilm reactor performance.

5. AI as a means for increasing biofilm reactor performance

5.1. Advances in AI methods for optimizing biofilm reactors

The optimization of biofilm reactor performance is evolving from using traditional experience-based methods to employing more robust and validated machine learning techniques with smart data treatment [162]. The level of microbial activity and the suitability of the operating conditions are key to the success of biofilm reactors, and assessing and evaluating reactor performance using advanced deep learning (DL) algorithms has considerably reduced the difficulties associated with understanding reactors' physical systems. Using DL algorithms consisting of different types of neural networks, including ANNs, can aid in optimizing the performance of biofilm reactors. ANNs have recently attracted attention for their ability to overcome the complexity of characteristic parameters and identify the relationships that link input data patterns to associated output data. Rather than using prior knowledge about the relationships between targeted responses, ANNs learn from real examples of reactor operations [163]. Thus, ANNs are becoming powerful tools for fitting experimental responses, predicting performance, and modeling biochemical processes [164,165].

Biofilm reactors hosting multi-species communities necessitate understanding the interactions among diverse microbial populations. Effectively managing these communities to achieve specific engineering objectives requires establishing predictive correlations between community structures and functional outcomes. AI plays a crucial role in this context, facilitating the generation of accurate predictions of microbial assemblages in various reactor types. The proliferation of sequencing data, coupled with increased computational capabilities, has propelled the development of AI methodologies capable of predicting community structures based on the operational parameters of biofilm reactors.

For instance, the inflow characteristics of microbial fuel cells have been used as ANN inputs to forecast the composition of microbial communities within biofilms [166], and the findings indicate that such an approach has significant potential in evaluating reactor performance and stability [166,167]. However, taxonomic consistency must be achieved before this approach can be applied to different biofilm reactor types. A shift toward evaluating systems at a functional level is crucial to enhance the scalability and applicability of AI approaches. Such an approach can effectively identify metabolic similarities across diverse taxa despite taxonomic differences, offering a more robust and scalable solution for managing multispecies biofilm reactors.

5.2. Algorithms used for biofilm reactor optimization

In addition to the general operating parameters of the reactor, such as the influent chemical oxygen demand (COD), hydraulic retention time (HRT), and substrate concentration [168,169], other characteristic parameters must also be inputted into ANNs to achieve a satisfactory prediction performance with a limited training set (Table 3). In one study, the wet/dry ratio and aeration/non-aeration ratio were set as the input parameters of a sequencing batch biofilm reactor combined with a vertical flow constructed wetland system to predict the NH_4^+-N, COD, total nitrogen (TN), and total phosphorus (TP) of the effluent, and a good generation ability was achieved with a root mean square error (RMSE) value less than 0.0782 and correlation coefficients all greater than 0.99 [165]. In another study that focused on biofilm reactors designed for heavy

Table 3
AI tools in biofilm reactors.

System type	AI tool	Input variable	Output	Prediction probability	Remark	Reference
MFC	ANN	Substrate type, wastewater parameters	Power density predictions, CE, and COD removal rate	16.01 ± 4.35%[a] 1.77 ± 0.57%[a] 4.07 ± 1.06%[a]	The relationships between wastewater characteristics, biofilm communities, and reactor performance were established.	[166]
MFC	ANN	Load resistance, cylinder material, electrodes locations, and cathode size	Output voltage	0.99662[b]	The relationship between voltage-current characteristics and performance parameters with feed water quality parameters was established.	[164]
MBBR	ANN	Influent feed, retention time, and influent COD	COD removed and effluent aniline	0.96[b], 0.042[c]	The relationship between operational parameters and effluent concentrations was established.	[169]
MBBR	ANN - Particle Swarm Optimization ANN - Levenberg Marquardt (ANN-LM)	COD surface area loading rate (SALR), COD volumetric loading rate (VLR), hydraulic retention time (HRT), and the initial concentration of 4-nonylphenol (4-NP) and 4-tert-octylphenol (4-t-OP)	The removal percentage of COD, 4-NP, and 4-t-OP	0.9989[b], 2.582×10^{-5c} 0.0043[d] 0.9997[b], 2.526e $\times$ 10^{-5c}, 0.0041[d]	The relationship between operational parameters and effluent concentrations was established.	[173]
FBR	ANN	pH, temperature (°C), feed flux (mL min^{-1}), substrate flow (mL min^{-1}), and HRT (h)	Removal efficiency of Co(II), Ni(II), Zn(II), and turbidity	>0.99[b]	pH and temperature were found to be the most important parameters.	[170]
FBR	Stacked denoising auto-encoders deep learning network model Backpropagation neural network support vector regression Extreme learning machine Gradient boosting decision tree	Concentrations of chemical oxygen demand (COD), ammonia (NH_4^+-N), and total nitrogen (TN) of biofilm system influent, concentrations of COD, NH_4^+-N, and TN of anoxic biofilm reactor effluent, influent flow, and reflux ratio of biofilm system	Concentrations of NH_4^+-N, TN, and COD of biofilm system effluent	0.94[d], 1.04[d], 4.8[d] 1.27[f], 1.26[f], 5.94[f] 53.6[g], 7.28[g], 13.29[g]	The Stacked denoising auto-encoders model demonstrated strong anti-interference capability and high predictive accuracy.	[174]
FBR	ANN Modified stover kincannon Evolutionary polynomial regression (EPR)	Influent COD, aeration rates, and operating run time	Effluent COD	0.95[b], 0.1[h]	Evolutionary polynomial regression provided a more interpretable model structure.	[168]
SBBR-VFCW	ANN	NH_4^+-N, COD and TP of the influent, DO, wet/dry ratio, and aeration/non-aeration ratio	NH_4^+-N, TN, COD, and TP of effluent	0.9948[b], 0.9995[b], 0.9972[b], 0.9982[b] 0.0718[c], 0.0782[c], 0.0568[c], 0.0565[c] 9.5178[e], 6.9872[e], 7.5291[e], 4.7045[e]	The relationship between influent parameters and effluent parameters was established.	[165]
MRBC	ANN Response surface methodology (RSM)	Disk rotational speed, membrane-to-disk gap, and organic loading rate	Membrane permeability	0.9982[b]	The ANN model more accurately captures nonlinear relationships between parameters than the RSM.	[171]

[a] Average percentage error.
[b] Correlation coefficient.
[c] Root mean square.
[d] Mean absolute error.
[e] Standard error of prediction.
[f] Root mean squared error.
[g] Mean relative error.
[h] Minimum normalized mean square error.

metal absorption, pH (a critical factor that affects metal mobility and speciation) was used as an input for an ANN and found to have a significant impact; optimal removal was achieved in a weak acid environment [170]. Similarly, the disk rotational speed and membrane-to-disk gap were optimized in membrane-rotatingbiological contactors (MRBCs) through an ANN to enhance membrane permeability [171]. While such optimization traditionally falls under the purview of response surface methodology (RSM), this approach can be limited by decreased prediction accuracy, particularly when dealing with nonlinear variable relationships [172]. ANNs, however, have exhibited robust capabilities in modeling complex nonlinear multivariate relationships, as evidenced by the higher R^2 values achieved compared to RSM in MRBC applications [171].

The choice of training algorithm also influences the efficacy of ANNs in optimizing biofilm reactors. Comparing the Levenberg−Marquardt algorithm and the particle swarm optimization meta-heuristic in MBBR applications revealed variable predictive accuracies dependent on the number of neurons and particles [173]. To overcome the high dependence of the number of samples and prevent them from tending to fall into local optima during the training process, a DL neural network was introduced. Compared with conventional ANNs, DL neural networks offer advantages, including considerable capacities to learn, undertake nonlinear mapping, and effectively and flexibly express highly variant nonlinear functions. When DL neural network prediction models were applied to biofilm reactors continuously treating domestic wastewater, RMSE values of up to 1.27, 1.26, and 5.94 were obtained for the predicted NH_4^+-N, TN, and COD, respectively [174].

Adding biofilm-related characteristic parameters as inputs can also significantly improve the accuracy of the prediction, and combining information on a biofilm's community structure and inflow characteristics may provide better predictions than using only substrate information [166]. In addition, including information on the fluid velocity and biofilm thickness (measured nondestructively via OCT) may allow a more accurate reflection of the hydrodynamic properties of the reactor [175]. However, the difficulties associated with obtaining such information about biofilms and the consequent use of more diverse biofilm parameters limit the output of models. In the future, the use of new *in situ* nondestructive detection methods for identifying key biofilm parameters may, in turn, allow more accurate modeling and predictions of biofilm reactor performance.

6. Future Outlook

The heterogeneous structure of biofilms challenges the traditional view of them as uniform porous media with a constant mass transfer coefficient. Elucidating the mechanisms responsible for forming these heterogeneous structures is a crucial direction for future biofilm research. Additionally, in terms of engineering applications, researchers face the challenge of identifying a convenient method for adjusting the structure of biofilms to achieve more efficient mass transfer and thereby enhance the performance of biofilm reactors for environmental and bioenergy applications. Developing a stable and periodic biofilm detachment technique is also key for optimizing mass transfer efficiency while maintaining the operational stability of biofilm reactors.

Advanced measurement techniques enable high-resolution characterization of biofilm structures and their microenvironments. By combining these methods with AI algorithms, researchers are now beginning to perform detailed quantitative assessments of biofilm matrices. Furthermore, the emergence of nondestructive analytical techniques, such as OCT, is resulting in new ways to study the dynamics of biofilms, while nanosensors show promise for real-time monitoring of biofilms despite challenges associated with potential interference.

The dynamics among reactors performance, biofilm structure and their microbial communities are complex, nonlinear, and time-variant. Hence, generating models that reflect these systems using traditional methods is challenging. The use of ANNs is a potential solution; however, the lack of suitable biofilm-related parameters hinders their optimal use. Nevertheless, the ongoing development of nondestructive online measurement techniques may, in the future, provide the data needed to improve machine learning models, allow the dynamic structure of biofilms to be captured, and contribute to the enhanced performance of reactors designed for environmental and bioenergy applications.

7. Conclusions

The mass transfer processes within biofilms critically shape the microenvironment and microbial activity, thereby significantly influencing biofilm reactors' performance. Understanding these mass transfer processes and biofilm microorganism-environment interactions is crucial for optimizing biofilm reactor performance. The development of advanced measurement techniques is aiding our understanding of the heterogeneous structure of biofilms down to the molecular level. In the future, it is anticipated that more efficient mass transfer will be achieved by developing systems that integrate characteristics from typical reactor designs and optimizing the biofilm architecture. Machine learning algorithms facilitate the extraction and prediction of biofilm-related information, opening new avenues for measuring and predicting biofilm reactor dynamics. Integrating advanced measurement techniques with AI is expected to enhance the quantitative assessment of biofilm matrices. Despite biofilm reactors being complex systems, using ANNs shows promise in modeling these systems. While there is a current lack of characteristic biofilm parameters, the future development of nondestructive measurement techniques will likely result in new data that can be used to improve the accuracy of machine learning models, understand the dynamic structure of biofilms, and optimize the performance of biofilm reactors.

CRediT authorship contribution statement

Huize Chen: Writing - Original Draft, Methodology, Investigation. **Ao Xia:** Writing - Review & Editing, Conceptualization. **Huchao Yan:** Methodology, Writing - Original Draft. **Yun Huang:** Methodology, Writing - Original Draft. **Xianqing Zhu:** Writing - Review & Editing. **Xun Zhu:** Project Administration. **Qiang Liao:** Supervision.

Declaration of competing interest

The authors declare that they have no known competing financial interests or personal relationships that could have appeared to influence the work reported in this paper.

Acknowledgments

This work was supported by the National Natural Science Foundation of China (Nos. 52022015, 52021004), the Natural Science Foundation of Chongqing (Nos. CSTB2023NSCQ-JQX0005, cstc2021ycjh - bgzxm0160), and the Fundamental Research Funds for the Central Universities (No. 2022ZFJH04).

Appendix A. Supplementary data

Supplementary data to this article can be found online at https://doi.org/10.1016/j.ese.2024.100480.

References

[1] S. Dale, BP Statistical Review of World Energy, BP Plc, London, United Kingdom, 2021, pp. 14–16.
[2] H. Heidari, et al., Review of global energy trends towards 2040 and recommendations for Iran oil and gas sector, Int. J. Environ. Sci. Technol. 19 (2022) 8007–8018, https://doi.org/10.1007/s13762-022-03963-w.
[3] S. Kanwal, et al., An integrated future approach for the energy security of Pakistan: replacement of fossil fuels with syngas for better environment and socio-economic development, Renew. Sustain. Energy Rev. 156 (2022) 111978, https://doi.org/10.1016/j.rser.2021.111978.
[4] N. Tripathi, et al., Biomass waste utilisation in low-carbon products: harnessing a major potential resource, npj Clim. Atmos. Sci. 2 (2019) 35, https://doi.org/10.1038/s41612-019-0093-5.
[5] V.P. Aravani, et al., Agricultural and livestock sector's residues in Greece & China: comparative qualitative and quantitative characterization for assessing their potential for biogas production, Renew. Sustain. Energy Rev. 154 (2022) 111821, https://doi.org/10.1016/j.rser.2021.111821.
[6] S. Nanda, F. Berruti, Municipal solid waste management and landfilling technologies: a review, Environ. Chem. Lett. 19 (2021) 1433–1456, https://doi.org/10.1007/s10311-020-01100-y.
[7] J. Escalante, et al., Pyrolysis of lignocellulosic, algal, plastic, and other biomass wastes for biofuel production and circular bioeconomy: a review of thermogravimetric analysis (TGA) approach, Renew. Sustain. Energy Rev. 169 (2022) 112914, https://doi.org/10.1016/j.rser.2022.112914.
[8] M. Das, et al., Metabolic engineering for enhancing microbial biosynthesis of advanced biofuels, Renew. Sustain. Energy Rev. 119 (2020) 109562, https://doi.org/10.1016/j.rser.2019.109562.
[9] A. Abdelfattah, et al., High-strength wastewater treatment using microbial biofilm reactor: a critical review, World J. Microbiol. Biotechnol. 36 (2020) 75, https://doi.org/10.1007/s11274-020-02853-y.
[10] H. Aqeel, et al., Drivers of bioaggregation from flocs to biofilms and granular sludge, Environ. Sci. Water. Res. Technol. 5 (2019) 2072–2089, https://doi.org/10.1039/C9EW00450E.
[11] C. Juntawang, et al., Entrapped cells-based-anaerobic membrane bioreactor treating domestic wastewater: performances, fouling, and bacterial community structure, Chemosphere 187 (2017) 147–155, https://doi.org/10.1016/j.chemosphere.2017.08.113.
[12] F. Morgan-Sagastume, Biofilm development, activity and the modification of carrier material surface properties in moving-bed biofilm reactors (MBBRs) for wastewater treatment, Crit. Rev. Environ. Sci. Technol. 48 (2018) 439–470, https://doi.org/10.1080/10643389.2018.1465759.
[13] P. Riegler, et al., Continuous conversion of CO_2/H_2 with *Clostridium aceticum* in biofilm reactors, Bioresour. Technol. 291 (2019) 121760, https://doi.org/10.1016/j.biortech.2019.121760.
[14] X. Sun, et al., Biochar facilitated bioprocessing and biorefinery for productions of biofuel and chemicals: a review, Bioresour. Technol. 295 (2020) 122252, https://doi.org/10.1016/j.biortech.2019.122252.
[15] Y. Wang, et al., Perspectives on the feasibility of using microalgae for industrial wastewater treatment, Bioresour. Technol. 222 (2016) 485–497, https://doi.org/10.1016/j.biortech.2016.09.106.
[16] A. Zainab, et al., Study on natural organic materials as biofilm carriers for the optimization of anaerobic digestion, Waste Biomass Valor 11 (2020) 2521–2531, https://doi.org/10.1007/s12649-019-00628-7.
[17] J. Zheng, et al., Microbial interactions play a keystone role in rapid anaerobic ammonium oxidation sludge proliferation and biofilm formation, Bioresour. Technol. 387 (2023) 129612, https://doi.org/10.1016/j.biortech.2023.129612.
[18] P.A. Wilderer, B.S. McSwain, The SBR and its biofilm application potentials, Water Sci. Technol. 50 (2004) 1–10, https://doi.org/10.2166/wst.2004.0596.
[19] C.-Y. Chen, S.-D. Chen, Biofilm characteristics in biological denitrification biofilm reactors, Water Sci. Technol. 41 (2000) 147–154, https://doi.org/10.2166/wst.2000.0438.
[20] L.-A. Philipp, et al., Beneficial applications of biofilms, Nat. Rev. Microbiol. 22 (2024) 276–290, https://doi.org/10.1038/s41579-023-00985-0.
[21] H. Odegaard, Innovations in wastewater treatment: the moving bed biofilm process, Water Sci. Technol. 53 (2006) 17–33, https://doi.org/10.2166/wst.2006.284.
[22] W.A. Cavalcante, et al., Stimulation and inhibition of direct interspecies electron transfer mechanisms within methanogenic reactors by adding magnetite and granular actived carbon, Chem. Eng. J. 415 (2021) 128882, https://doi.org/10.1016/j.cej.2021.128882.
[23] D. Johnravindar, et al., Supplementing granular activated carbon for enhanced methane production in anaerobic co-digestion of post-consumer substrates, Biomass Bioenergy 136 (2020) 105543, https://doi.org/10.1016/j.biombioe.2020.105543.
[24] L. Yang, et al., Continuous treatment of hydrothermal liquefaction wastewater in an anaerobic biofilm reactor: potential role of granular activated carbon, J. Clean. Prod. 276 (2020) 122836, https://doi.org/10.1016/j.jclepro.2020.122836.
[25] J. Liu, et al., Enhancing anaerobic digestion in anaerobic integrated floating fixed-film activated sludge (An-IFFAS) system using novel electron mediator suspended biofilm carriers, Water Res. 175 (2020) 115697, https://doi.org/10.1016/j.watres.2020.115697.
[26] X. Guo, et al., Revealing the role of conductive materials on facilitating direct interspecies electron transfer in syntrophic methanogenesis: a thermodynamic analysis, Energy 229 (2021) 120747, https://doi.org/10.1016/j.energy.2021.120747.
[27] D. Feng, et al., Continuous electromethanogenesis of propionate wastewater: effect of external voltage and hydraulic retention time, Chem. Eng. J. 454 (2023) 140267, https://doi.org/10.1016/j.cej.2022.140267.
[28] P. Landini, et al., Molecular mechanisms of compounds affecting bacterial biofilm formation and dispersal, Appl. Microbiol. Biotechnol. 86 (2010) 813–823, https://doi.org/10.1007/s00253-010-2468-8.
[29] C. Berne, et al., Bacterial adhesion at the single-cell level, Nat. Rev. Microbiol. 16 (2018) 616–627, https://doi.org/10.1038/s41579-018-0057-5.
[30] H.C. Flemming, S. Wuertz, Bacteria and archaea on Earth and their abundance in biofilms, Nat. Rev. Microbiol. 17 (2019) 247–260, https://doi.org/10.1038/s41579-019-0158-9.
[31] H.C. Flemming, J. Wingender, The biofilm matrix, Nat. Rev. Microbiol. 8 (2010) 623–633, https://doi.org/10.1038/nrmicro2415.
[32] K.P. Rumbaugh, K. Sauer, Biofilm dispersion, Nat. Rev. Microbiol. 18 (2020) 571–586, https://doi.org/10.1038/s41579-020-0385-0.
[33] M.E. Davey, G.A. O'Toole, Microbial biofilms: from ecology to molecular genetics, Microbiol. Mol. Biol. Rev. 64 (2000) 847–867, https://doi.org/10.1128/mmbr.64.4.847-867.2000.
[34] W. Zhao, et al., Extracellular polymeric substances—antibiotics interaction in activated sludge: a review, Environ. Sci. Ecotechnol. 13 (2023) 100212, https://doi.org/10.1016/j.ese.2022.100212.
[35] V. Krasňan, et al., Immobilization of cells and enzymes to LentiKats, Appl. Microbiol. Biotechnol. 100 (2016) 2535–2553, https://doi.org/10.1007/s00253-016-7283-4.
[36] H. Horn, S. Lackner, Modeling of biofilm systems: a review, Prod. Biofilms (2014) 53–76.
[37] M.C.M. van Loosdrecht, et al., Mathematical modelling of biofilm structures, Antonie Leeuwenhoek 81 (2002) 245–256, https://doi.org/10.1023/A:1020527020464.
[38] H.-C. Flemming, et al., The biofilm matrix: multitasking in a shared space, Nat. Rev. Microbiol. (2022), https://doi.org/10.1038/s41579-022-00791-0.
[39] V. Dunsing, et al., Purely polysaccharide-based biofilm matrix provides size-selective diffusion barriers for nanoparticles and bacteriophages, Biomacromolecules 20 (2019) 3842–3854, https://doi.org/10.1021/acs.biomac.9b00938.
[40] J.N. Wilking, et al., Liquid transport facilitated by channels in *Bacillus subtilis* biofilms, Proc. Natl. Acad. Sci. U.S.A. 110 (2013) 848–852, https://doi.org/10.1073/pnas.1216376110.
[41] H.L. Røder, et al., Unravelling interspecies interactions across heterogeneities in complex biofilm communities, Environ. Microbiol. 22 (2020) 5–16, https://doi.org/10.1111/1462-2920.14834.
[42] A. Xia, et al., Mathematical modeling of intercellular interactions within the biofilm, Trends Microbiol. 30 (2022) 925–929, https://doi.org/10.1016/j.tim.2022.07.005.
[43] O. Wanner, W. Gujer, A multispecies biofilm model, Biotechnol. Bioeng. 28 (1986) 314–328, https://doi.org/10.1002/bit.260280304.
[44] P.S. Stewart, Diffusion in biofilms, J. Bacteriol. 185 (2003) 1485–1491, https://doi.org/10.1128/jb.185.5.1485-1491.2003.
[45] M.P. Herrling, et al., NMR investigation of water diffusion in different biofilm structures, Biotechnol. Bioeng. 114 (2017) 2857–2867, https://doi.org/10.1002/bit.26392.
[46] X. Chen, et al., Model predicted N_2O production from membrane-aerated biofilm reactor is greatly affected by biofilm property settings, Chemosphere 281 (2021) 130861, https://doi.org/10.1016/j.chemosphere.2021.130861.
[47] C. Picard, et al., Mass transfer in a membrane aerated biofilm, Water Res. 46 (2012) 4761–4769, https://doi.org/10.1016/j.watres.2012.05.056.
[48] M.R. Mattei, et al., Continuum and discrete approach in modeling biofilm development and structure: a review, J. Math. Biol. 76 (2018) 945–1003, https://doi.org/10.1007/s00285-017-1165-y.
[49] A. Keren-Paz, et al., Micro-CT X-ray imaging exposes structured diffusion barriers within biofilms, npj Biofilms Microbomes 4 (2018) 8, https://doi.org/10.1038/s41522-018-0051-8.
[50] G. You, et al., Insights into spatial effects of ceria nanoparticles on oxygen mass transfer in wastewater biofilms: interfacial microstructure, in-situ microbial activity and metabolism regulation mechanism, Water Res. 176 (2020) 115731, https://doi.org/10.1016/j.watres.2020.115731.
[51] J. Yang, et al., Sensitivity to oxygen in microbial electrochemical systems biofilms, iScience 13 (2019) 163–172, https://doi.org/10.1016/j.isci.2019.01.022.
[52] J.W. Hart, et al., Microrheology and spatial heterogeneity of *Staphylococcus aureus* biofilms modulated by hydrodynamic shear and biofilm-degrading enzymes, Langmuir 35 (2019) 3553–3561, https://doi.org/10.1021/acs.langmuir.8b04252.
[53] H. Liu, et al., Bacterial community structure and activity of sulfate reducing bacteria in a membrane aerated biofilm analyzed by microsensor and

molecular techniques, Biotechnol. Bioeng. 111 (2014) 2155–2162, https://doi.org/10.1002/bit.25277.
[54] T. Shoji, et al., Influence of the flow velocity on membrane-aerated biofilm reactors: application of a rotating disk for local flow control, Biochem. Eng. J. 164 (2020) 107771, https://doi.org/10.1016/j.bej.2020.107771.
[55] Y. Pechaud, et al., Modelling biofilm development: the importance of considering the link between EPS distribution, detachment mechanisms and physical properties, Water Res. 250 (2024) 120985, https://doi.org/10.1016/j.watres.2023.120985.
[56] J. Yang, et al., Shear stress affects biofilm structure and consequently current generation of bioanode in microbial electrochemical systems (MESs), Front. Microbiol. 10 (2019) 398, https://doi.org/10.3389/fmicb.2019.00398.
[57] R.C. Pessotti, et al., High spatial resolution imaging mass spectrometry reveals chemical heterogeneity across bacterial microcolonies, Anal. Chem. 91 (2019) 14818–14823, https://doi.org/10.1021/acs.analchem.9b03909.
[58] J. Ye, et al., A facile and fast strategy for cathodic electroactive-biofilm assembly via magnetic nanoparticle bioconjugation, Biosens. Bioelectron. 190 (2021) 113464, https://doi.org/10.1016/j.bios.2021.113464.
[59] B. Taşkan, et al., New quorum quenching bacteria for controlling biofilm thickness in the membrane aerated biofilm reactor, Process Saf. Environ. Protect. 165 (2022) 57–65, https://doi.org/10.1016/j.psep.2022.06.056.
[60] B. Taşkan, et al., Effective biofilm control in a membrane biofilm reactor using a quenching bacterium (*Rhodococcus sp.* BH4), Biotechnol. Bioeng. 117 (2020) 1012–1023, https://doi.org/10.1002/bit.27259.
[61] M. Aybar, et al., Predation creates unique void layer in membrane-aerated biofilms, Water Res. 149 (2019) 232–242, https://doi.org/10.1016/j.watres.2018.10.084.
[62] J. Ye, et al., Solar-driven methanogenesis with ultrahigh selectivity by turning down H_2 production at biotic-abiotic interface, Nat. Commun. 13 (2022) 6612, https://doi.org/10.1038/s41467-022-34423-1.
[63] C. Tan, et al., Effects of tourmaline on nitrogen removal performance and biofilm structures in the sequencing batch biofilm reactor, J. Environ. Sci. 67 (2018) 127–135, https://doi.org/10.1016/j.jes.2017.08.012.
[64] J.R. Lawrence, et al., In situ evidence for metabolic and chemical microdomains in the structured polymer matrix of bacterial microcolonies, FEMS Microbiol. Ecol. 92 (2016) fiw183, https://doi.org/10.1093/femsec/fiw183.
[65] B.R. Dhar, et al., Microbial activity influences electrical conductivity of biofilm anode, Water Res. 127 (2017) 230–238, https://doi.org/10.1016/j.watres.2017.10.028.
[66] S. Fulaz, et al., Ratiometric imaging of the in situ pH distribution of biofilms by use of fluorescent mesoporous silica nanosensors, ACS Appl. Mater. Interfaces 11 (2019) 32679–32688, https://doi.org/10.1021/acsami.9b09978.
[67] J. Yan, et al., Mechanical instability and interfacial energy drive biofilm morphogenesis, Elife 8 (2019) e43920, https://doi.org/10.7554/eLife.43920.
[68] P. Liu, et al., Spatial variation of electrical conductance in electrochemically active biofilm growing on interdigitated microelectrode array, J. Power Sources 491 (2021) 229615, https://doi.org/10.1016/j.jpowsour.2021.229615.
[69] G. Yang, et al., Anode potentials regulate *Geobacter* biofilms: new insights from the composition and spatial structure of extracellular polymeric substances, Water Res. 159 (2019) 294–301, https://doi.org/10.1016/j.watres.2019.05.027.
[70] F.J. Otero, et al., Evidence of a streamlined extracellular electron transfer pathway from biofilm structure, metabolic stratification, and long-range electron transfer parameters, Appl. Environ. Microbiol. 87 (2021) e00706–e00721, https://doi.org/10.1128/AEM.00706-21.
[71] H. Wang, et al., In situ tuning the structure of *Geobacter* biofilm for bioelectricity enhancement, Environ. Sci. Technol. Lett. 11 (2024) 106–113, https://doi.org/10.1021/acs.estlett.3c00783.
[72] C. Li, et al., Assessing the influence of biofilm surface roughness on mass transfer by combining optical coherence tomography and two-dimensional modeling, Biotechnol. Bioeng. 113 (2016) 989–1000, https://doi.org/10.1002/bit.25868.
[73] L. Fortunato, et al., In-situ assessment of biofilm formation in submerged membrane system using optical coherence tomography and computational fluid dynamics, J. Membr. Sci. 521 (2017) 84–94, https://doi.org/10.1016/j.memsci.2016.09.004.
[74] B. Manz, et al., Measuring local flow velocities and biofilm structure in biofilm systems with Magnetic Resonance Imaging (MRI), Biotechnol. Bioeng. 84 (2003) 424–432, https://doi.org/10.1002/bit.10782.
[75] Y. Guo, et al., Monitoring stratification of anode biofilms in bioelectrochemical laminar flow reactors using flow cytometry, Environ. Sci. Ecotechnol. 4 (2020) 100062, https://doi.org/10.1016/j.ese.2020.100062.
[76] H. Cao, et al., Revealing region-specific biofilm viscoelastic properties by means of a micro-rheological approach, npj Biofilms Microbomes 2 (2016) 5, https://doi.org/10.1038/s41522-016-0005-y.
[77] H. Wang, et al., Influence of fimbriae on bacterial adhesion and viscoelasticity and correlations of the two properties with biofilm formation, Langmuir 33 (2017) 100–106, https://doi.org/10.1021/acs.langmuir.6b03764.
[78] X. Liu, et al., Flagella act as *Geobacter* biofilm scaffolds to stabilize biofilm and facilitate extracellular electron transfer, Biosens. Bioelectron. 146 (2019) 111748, https://doi.org/10.1016/j.bios.2019.111748.
[79] R. Hartmann, et al., Emergence of three-dimensional order and structure in growing biofilms, Nat. Phys. 15 (2019) 251–256, https://doi.org/10.1038/s41567-018-0356-9.
[80] P. Desmond, et al., Linking composition of extracellular polymeric substances (EPS) to the physical structure and hydraulic resistance of membrane biofilms, Water Res. 132 (2018) 211–221, https://doi.org/10.1016/j.watres.2017.12.058.
[81] R.B. Möhle, et al., Structure and shear strength of microbial biofilms as determined with confocal laser scanning microscopy and fluid dynamic gauging using a novel rotating disc biofilm reactor, Biotechnol. Bioeng. 98 (2007) 747–755, https://doi.org/10.1002/bit.21448.
[82] Y. Xue, et al., Uncovering the molecular composition and architecture of the *Bacillus subtilis* biofilm via solid-state NMR spectroscopy, J. Am. Chem. Soc. 146 (2024) 11906–11923, https://doi.org/10.1021/jacs.4c00889.
[83] H.-C. Liou, et al., Layered viscoelastic properties of granular biofilms, Water Res. 202 (2021) 117394, https://doi.org/10.1016/j.watres.2021.117394.
[84] C. Picioreanu, et al., Determination of mechanical properties of biofilms by modelling the deformation measured using optical coherence tomography, Water Res. 145 (2018) 588–598, https://doi.org/10.1016/j.watres.2018.08.070.
[85] J.P. Pavissich, et al., Spatial distribution of mechanical properties in *Pseudomonas aeruginosa* biofilms, and their potential impacts on biofilm deformation, Biotechnol. Bioeng. 118 (2021) 1545–1556, https://doi.org/10.1002/bit.27671.
[86] M. Relucenti, et al., Microscopy methods for biofilm imaging: focus on SEM and VP-SEM Pros and Cons, Biol. 10 (2021) 51, https://doi.org/10.3390/biology10010051.
[87] M. Bossù, et al., Morpho-chemical observations of human deciduous teeth enamel in response to biomimetic toothpastes treatment, Materials 13 (2020) 1803, https://doi.org/10.3390/ma13081803.
[88] L.M. Joubert, et al., Visualization of *Aspergillus fumigatus* biofilms with scanning electron microscopy and variable pressure-scanning electron microscopy: a comparison of processing techniques, J. Microbiol. Methods 132 (2017) 46–55, https://doi.org/10.1016/j.mimet.2016.11.002.
[89] M. Alhede, et al., Combination of microscopic techniques reveals a comprehensive visual impression of biofilm structure and composition, FEMS Microbiol. Immunol. 65 (2012) 335–342, https://doi.org/10.1111/j.1574-695X.2012.00956.x.
[90] A. Harimawan, et al., Adhesion of *B. subtilis* spores and vegetative cells onto stainless steel – DLVO theories and AFM spectroscopy, J. Colloid Interface Sci. 405 (2013) 233–241, https://doi.org/10.1016/j.jcis.2013.05.031.
[91] C.T. Kreis, R.M.A. Sullan, Interfacial nanomechanical heterogeneity of the E. coli biofilm matrix, Nanoscale 12 (2020) 16819–16830, https://doi.org/10.1039/D0NR03646C.
[92] B. Kundukad, et al., Mechanical properties of the superficial biofilm layer determine the architecture of biofilms, Soft Matter 12 (2016) 5718–5726, https://doi.org/10.1039/C6SM00687F.
[93] L.C. Powell, et al., Quantifying the effects of antibiotic treatment on the extracellular polymer network of antimicrobial resistant and sensitive biofilms using multiple particle tracking, npj Biofilms and Microbiomes 7 (2021) 13, https://doi.org/10.1038/s41522-020-00172-6.
[94] O. Lieleg, et al., Characterization of particle translocation through mucin hydrogels, Biophys. J. 98 (2010) 1782–1789, https://doi.org/10.1016/j.bpj.2010.01.012.
[95] Q. Xu, et al., Nanoparticle diffusion in, and microrheology of, the bovine vitreous ex vivo, J. Contr. Release 167 (2013) 76–84, https://doi.org/10.1016/j.jconrel.2013.01.018.
[96] T.R. Neu, J.R. Lawrence, Innovative techniques, sensors, and approaches for imaging biofilms at different scales, Trends Microbiol. 23 (2015) 233–242, https://doi.org/10.1016/j.tim.2014.12.010.
[97] N. Nagaraja, et al., Investigation of compounds that degrade biofilm polysaccharides on reverse osmosis membranes from a full scale desalination plant to alleviate biofouling, Desalination 403 (2017) 88–96, https://doi.org/10.1016/j.desal.2016.06.002.
[98] C. Gonzalez-Machado, et al., Visualization and quantification of the cellular and extracellular components of *Salmonella Agona* biofilms at different stages of development, PLoS One 13 (2018) e0200011, https://doi.org/10.1371/journal.pone.0200011.
[99] N. Peng, et al., The exopolysaccharide-eDNA interaction modulates 3D architecture of *Bacillus subtilis* biofilm, BMC Microbiol. 20 (2020) 115, https://doi.org/10.1186/s12866-020-01789-5.
[100] M.Y. Chen, et al., Staining of extracellular polymeric substances and cells in bioaggregates, Appl. Microbiol. Biotechnol. 75 (2007) 467–474, https://doi.org/10.1007/s00253-006-0816-5.
[101] G. Ren, et al., Graphite-assisted electro-fermentation methanogenesis: spectroelectrochemical and microbial community analyses of cathode biofilms, Bioresour. Technol. 269 (2018) 74–80, https://doi.org/10.1016/j.biortech.2018.08.078.
[102] D.N. Hohne, et al., Flexible microfluidic device for mechanical property characterization of soft viscoelastic solids such as bacterial biofilms, Langmuir 25 (2009) 7743–7751, https://doi.org/10.1021/la803413x.
[103] H.C. Flemming, et al., Biofilms: an emergent form of bacterial life, Nat. Rev. Microbiol. 14 (2016) 563–575, https://doi.org/10.1038/nrmicro.2016.94.
[104] M. Wagner, et al., Investigation of the mesoscale structure and volumetric features of biofilms using optical coherence tomography, Biotechnol. Bioeng. 107 (2010) 844–853, https://doi.org/10.1002/bit.22864.
[105] L. Fortunato, T. Leiknes, In-situ biofouling assessment in spacer filled channels using optical coherence tomography (OCT): 3D biofilm thickness

mapping, Bioresour. Technol. 229 (2017) 231–235, https://doi.org/10.1016/j.biortech.2017.01.021.
[106] S. Fabbri, et al., A marine biofilm flow cell for in situ screening marine fouling control coatings using optical coherence tomography, Ocean Eng. 170 (2018) 321–328, https://doi.org/10.1016/j.oceaneng.2018.10.030.
[107] C. Li, et al., Investigating biofilm structure developing on carriers from lab-scale moving bed biofilm reactors based on light microscopy and optical coherence tomography, Bioresour. Technol. 200 (2016) 128–136, https://doi.org/10.1016/j.biortech.2015.10.013.
[108] L. Gierl, et al., An open-source robotic platform that enables automated monitoring of replicate biofilm cultivations using optical coherence tomography, npj Biofilms and Microbiomes 6 (2020) 18, https://doi.org/10.1038/s41522-020-0129-y.
[109] F. Blauert, et al., Time-resolved biofilm deformation measurements using optical coherence tomography, Biotechnol. Bioeng. 112 (2015) 1893–1905, https://doi.org/10.1002/bit.25590.
[110] J. Hou, et al., Bacterial density and biofilm structure determined by optical coherence tomography, Sci. Rep. 9 (2019) 9794, https://doi.org/10.1038/s41598-019-46196-7.
[111] S.D. Molenaar, et al., In situ biofilm quantification in bioelectrochemical systems by using optical coherence tomography, ChemSusChem 11 (2018) 2171–2178, https://doi.org/10.1002/cssc.201800589.
[112] G. Hidalgo, et al., Functional tomographic fluorescence imaging of pH microenvironments in microbial biofilms by use of silica nanoparticle sensors, Appl. Environ. Microbiol. 75 (2009) 7426–7435, https://doi.org/10.1128/aem.01220-09.
[113] K.J. Cash, et al., Optical drug monitoring: photoacoustic imaging of nanosensors to monitor therapeutic lithium in vivo, ACS Nano 9 (2015) 1692–1698, https://doi.org/10.1021/nn5064858.
[114] M.P. Jewell, et al., Luminescent nanosensors for ratiometric monitoring of three-dimensional oxygen gradients in laboratory and clinical *Pseudomonas aeruginosa* biofilms, Appl. Environ. Microbiol. 85 (2019) e01116–e01119, https://doi.org/10.1128/AEM.01116-19.
[115] B. Hollmann, et al., Fluorescent nanosensors reveal dynamic pH gradients during biofilm formation, npj Biofilms Microbomes 7 (2021) 50, https://doi.org/10.1038/s41522-021-00221-8.
[116] G.-R. Tan, et al., pH-responsive hybrid nanoparticles for imaging spatiotemporal pH changes in biofilm-dentin microenvironments, ACS Appl. Mater. Interfaces 13 (2021) 46247–46259, https://doi.org/10.1021/acsami.1c11162.
[117] J. Dias, et al., Influence of carrier media physical properties on start-up of moving attached growth systems, Bioresour. Technol. 266 (2018) 463–471, https://doi.org/10.1016/j.biortech.2018.06.096.
[118] S. Ragi, et al., Artificial intelligence-driven image analysis of bacterial cells and biofilms, IEEE ACM Trans. Comput. Biol. Bioinf (2021), https://doi.org/10.1109/TCBB.2021.3138304, 1-1.
[119] P.-C. Wong, et al., Detection and identification of the stages of DH5-alpha *Escherichia coli* biofilm formation on metal by using an artificial intelligence system, Microsc. Microanal. 27 (2021) 1218–1225, https://doi.org/10.1017/S1431927621012472.
[120] A. Buetti-Dinh, et al., Deep neural networks outperform human expert's capacity in characterizing bioleaching bacterial biofilm composition, Biotechnol. Rep. 22 (2019) e00321, https://doi.org/10.1016/j.btre.2019.e00321.
[121] H. Asgharnejad, et al., Biomass quantification and 3-D topography reconstruction of microalgal biofilms using digital image processing, Algal Res. 55 (2021) 102243, https://doi.org/10.1016/j.algal.2021.102243.
[122] M.J. Schulte, et al., A high gas fraction, reduced power, syngas bioprocessing method demonstrated with a *Clostridium ljungdahlii* OTA1 paper biocomposite, Biotechnol. Bioeng. 113 (2016) 1913–1923, https://doi.org/10.1002/bit.25966.
[123] P.C. Munasinghe, S.K. Khanal, Syngas fermentation to biofuel: evaluation of carbon monoxide mass transfer and analytical modeling using a composite hollow fiber (CHF) membrane bioreactor, Bioresour. Technol. 122 (2012) 130–136, https://doi.org/10.1016/j.biortech.2012.03.053.
[124] M.S. Rana, S.K. Prajapati, Mixotrophic microalgal-biofilm reactor augmenting biomass and biofuel productivity, Bioresour. Technol. 356 (2022) 127306, https://doi.org/10.1016/j.biortech.2022.127306.
[125] M. Safari, et al., Biohydrogen production from diluted-acid hydrolysate of rice straw in a continuous anaerobic packed bed biofilm reactor, Int. J. Hydrogen Energy 47 (2022) 5879–5890, https://doi.org/10.1016/j.ijhydene.2021.11.222.
[126] A.G. Mari, et al., Biohydrogen and biomethane production from cassava wastewater in a two-stage anaerobic sequencing batch biofilm reactor, Int. J. Hydrogen Energy 45 (2020) 5165–5174, https://doi.org/10.1016/j.ijhydene.2019.07.054.
[127] Y. Shen, et al., Syngas fermentation of *Clostridium carboxidivoran* P7 in a hollow fiber membrane biofilm reactor: evaluating the mass transfer coefficient and ethanol production performance, Biochem. Eng. J. 85 (2014) 21–29, https://doi.org/10.1016/j.bej.2014.01.010.
[128] M.B. Jensen, et al., Selecting carrier material for efficient biomethanation of industrial biogas-CO_2 in a trickle-bed reactor, J. CO_2 Util. 51 (2021) 101611, https://doi.org/10.1016/j.jcou.2021.101611.
[129] R.B. Carneiro, et al., Two-phase (acidogenic-methanogenic) anaerobic fixed bed biofilm reactor enhances the biological domestic sewage treatment: perspectives for recovering bioenergy and value-added by-products, J. Environ. Manag. 317 (2022) 115388, https://doi.org/10.1016/j.jenvman.2022.115388.
[130] P. Ghofrani-Isfahani, et al., Ex-situ biogas upgrading in thermophilic trickle bed reactors packed with micro-porous packing materials, Chemosphere 296 (2022) 133987, https://doi.org/10.1016/j.chemosphere.2022.133987.
[131] Y. Shen, et al., Enhancing mass transfer and ethanol production in syngas fermentation of *Clostridium carboxidivorans* P7 through a monolithic biofilm reactor, Appl. Energy 136 (2014) 68–76, https://doi.org/10.1016/j.apenergy.2014.08.117.
[132] M.T. Kreutzer, et al., Multiphase monolith reactors: chemical reaction engineering of segmented flow in microchannels, Chem. Eng. Sci. 60 (2005) 5895–5916, https://doi.org/10.1016/j.ces.2005.03.022.
[133] A. Sathish, et al., A novel bulk-gas-to-atomized-liquid reactor for enhanced mass transfer efficiency and its application to syngas fermentation, Chem. Eng. J. 370 (2019) 60–70, https://doi.org/10.1016/j.cej.2019.03.183.
[134] W. Sokół, et al., Biological wastewater treatment in the inverse fluidised bed reactor, Chem. Eng. J. 150 (2009) 63–68, https://doi.org/10.1016/j.cej.2008.12.021.
[135] H. Fukuda, J.A. ASENJO, J.C. MERCHUK, Immobilized microorganism bioreactors, Bioreactor system design (1994) 339–375.
[136] M.J. Nelson, et al., Fluidized-bed bioreactor applications for biological wastewater treatment: a review of research and developments, Engineering 3 (2017) 330–342, https://doi.org/10.1016/J.ENG.2017.03.021.
[137] H.-Y. Ren, et al., Carrier modification and its application in continuous photo-hydrogen production using anaerobic fluidized bed photo-reactor, GCB Bioenergy 6 (2014) 599–605, https://doi.org/10.1111/gcbb.12073.
[138] C. Cisneros-Pérez, et al., Effect of inoculum pretreatment on the microbial community structure and its performance during dark fermentation using anaerobic fluidized-bed reactors, Int. J. Hydrogen Energy 42 (2017) 9589–9599, https://doi.org/10.1016/j.ijhydene.2017.03.157.
[139] P. Sonkar, et al., Chapter 2 - moving bed biofilm reactors, in: M.P. Shah, S. Rodriguez-Couto (Eds.), Membrane-Based Hybrid Processes for Wastewater Treatment, Elsevier, 2021, pp. 13–23, https://doi.org/10.1016/B978-0-12-823804-2.00019-7.
[140] A. Sinharoy, K. Pakshirajan, Methane free biohydrogen production from carbon monoxide using a continuously operated moving bed biofilm reactor, Int. J. Hydrogen Energy 46 (2021) 306–313, https://doi.org/10.1016/j.ijhydene.2020.09.250.
[141] Y. Shen, et al., Syngas fermentation by *Clostridium carboxidivorans* P7 in a horizontal rotating packed bed biofilm reactor with enhanced ethanol production, Appl. Energy 187 (2017) 585–594, https://doi.org/10.1016/j.apenergy.2016.11.084.
[142] V. Sivalingam, C. Dinamarca, High pressure moving bed biofilm reactor for syngas fermentation, Chem. Eng. Trans. 86 (2021) 1483–1488, https://doi.org/10.3303/CET2186248.
[143] X. Wang, et al., Morphological image analysis of biofilm evolution with quantitative analysis in a moving bed biofilm reactor, Sci. Total Environ. 856 (2023) 159199, https://doi.org/10.1016/j.scitotenv.2022.159199.
[144] S. Sarkar, et al., Enhanced production of antimicrobial compounds by three salt-tolerant actinobacterial strains isolated from the sundarbans in a niche-mimic bioreactor, Mar. Biotechnol. 10 (2008) 518–526, https://doi.org/10.1007/s10126-008-9090-0.
[145] W. Blanken, et al., Biofilm growth of *Chlorella sorokiniana* in a rotating biological contactor based photobioreactor, Biotechnol. Bioeng. 111 (2014) 2436–2445, https://doi.org/10.1002/bit.25301.
[146] R. Nerenberg, The membrane-biofilm reactor (MBfR) as a counter-diffusional biofilm process, Curr. Opin. Biotechnol. 38 (2016) 131–136, https://doi.org/10.1016/j.copbio.2016.01.015.
[147] G. Pratofiorito, et al., A membrane biofilm reactor for hydrogenotrophic methanation, Bioresour. Technol. 321 (2021) 124444, https://doi.org/10.1016/j.biortech.2020.124444.
[148] C.T. Kinh, et al., Identification of hotspots for NO and N2O production and consumption in counter- and co-diffusion biofilms for simultaneous nitrification and denitrification, Bioresour. Technol. 245 (2017) 318–324, https://doi.org/10.1016/j.biortech.2017.08.051.
[149] M.W. Reij, et al., Membrane bioreactors for waste gas treatment, J. Biotechnol. 59 (1998) 155–167, https://doi.org/10.1016/S0168-1656(97)00169-7.
[150] H. Tao, et al., Preparation of PDMS and PDMS-UiO-66 oxygen-rich membranes and modules for membrane-aerated biofilm reactors, Water Sci. Technol. 89 (2024) 873–886, https://doi.org/10.2166/wst.2024.043.
[151] F. Zhang, et al., Fatty acids production from hydrogen and carbon dioxide by mixed culture in the membrane biofilm reactor, Water Res. 47 (2013) 6122–6129, https://doi.org/10.1016/j.watres.2013.07.033.
[152] M.P. Elisiário, et al., Membrane bioreactors for syngas permeation and fermentation, Crit. Rev. Biotechnol. 42 (2022) 856–872, https://doi.org/10.1080/07388551.2021.1965952.
[153] K.-K. Wu, et al., Recovery of methane and acetate during ex-situ biogas upgrading via novel dual-membrane aerated biofilm reactor, Bioresour. Technol. 382 (2023) 129181, https://doi.org/10.1016/j.biortech.2023.129181.
[154] H.-J. Wang, et al., Tunable production of ethanol and acetate from synthesis gas by mesophilic mixed culture fermentation in a hollow fiber membrane biofilm reactor, J. Clean. Prod. 187 (2018) 165–170, https://doi.org/10.1016/j.jclepro.2018.03.193.
[155] Y. Yuan, et al., Electrochemical surface plasmon resonance fiber-optic sensor:

in situ detection of electroactive biofilms, Anal. Chem. 88 (2016) 7609−7616, https://doi.org/10.1021/acs.analchem.6b01314.
[156] B. Wang, et al., Bioenergy recovery from wastewater accelerated by solar power: intermittent electro-driving regulation and capacitive storage in biomass, Water Res. 175 (2020) 115696, https://doi.org/10.1016/j.watres.2020.115696.
[157] W. Cai, et al., An electrolytic-hydrogen-fed moving bed biofilm reactor for efficient microbial electrosynthesis of methane from CO_2, Chem. Eng. J. 428 (2022) 132093, https://doi.org/10.1016/j.cej.2021.132093.
[158] L. Luo, et al., Assistant role of bioelectrode on methanogenic reactor under ammonia stress, Bioresour. Technol. 217 (2016) 72−81, https://doi.org/10.1016/j.biortech.2016.02.092.
[159] J. Yu, et al., Effect of applied voltage and temperature on methane production and microbial community in microbial electrochemical anaerobic digestion systems treating swine manure, J. Ind. Microbiol. Biotechnol. 46 (2019) 911−923, https://doi.org/10.1007/s10295-019-02182-6.
[160] E. Zkeri, et al., Comparing the use of a two-stage MBBR system with a methanogenic MBBR coupled with a microalgae reactor for medium-strength dairy wastewater treatment, Bioresour. Technol. 323 (2021) 124629, https://doi.org/10.1016/j.biortech.2020.124629.
[161] C. Xiao, et al., Photocatalytic synergistic biofilms enhance tetracycline degradation and conversion, Environ. Sci. Ecotechnol. 14 (2023) 100234, https://doi.org/10.1016/j.ese.2022.100234.
[162] Z. Wang, et al., The role of machine learning to boost the bioenergy and biofuels conversion, Bioresour. Technol. 343 (2022) 126099, https://doi.org/10.1016/j.biortech.2021.126099.
[163] H.C. Yu, et al., Comparison of artificial neural networks and response surface methodology towards an efficient ultrasound-assisted extraction of chlorogenic acid from Lonicera japonica, Molecules 24 (2019) 2304, https://doi.org/10.3390/molecules24122304, 10.3390/molecules24122304.
[164] M.-A. Tsompanas, et al., Artificial neural network simulating microbial fuel cells with different membrane materials and electrode configurations, J. Power Sources 436 (2019) 226832, https://doi.org/10.1016/j.jpowsour.2019.226832.
[165] Y.-M. Guo, et al., An integrated treatment of domestic wastewater using sequencing batch biofilm reactor combined with vertical flow constructed wetland and its artificial neural network simulation study, Ecol. Eng. 64 (2014) 18−26, https://doi.org/10.1016/j.ecoleng.2013.12.040.
[166] K.L. Lesnik, H. Liu, Predicting microbial fuel cell biofilm communities and bioreactor performance using artificial neural networks, Environ. Sci. Technol. 51 (2017) 10881−10892, https://doi.org/10.1021/acs.est.7b01413.
[167] A. Dutta, et al., Machine learning predicts biogeochemistry from microbial community structure in a complex model system, Microbiol. Spectr. 10 (2022), https://doi.org/10.1128/spectrum.01909-21.
[168] S.A. Kordkandi, L. Berardi, Comparing new perspective of hybrid approach and conventional kinetic modelling techniques of a submerged biofilm reactor performance, Biochem. Eng. J. 103 (2015) 170−176, https://doi.org/10.1016/j.bej.2015.07.007.
[169] M. Delnavaz, et al., Prediction of moving bed biofilm reactor (MBBR) performance for the treatment of aniline using artificial neural networks (ANN), J. Hazard Mater. 179 (2010) 769−775, https://doi.org/10.1016/j.jhazmat.2010.03.069.
[170] A.K. Maurya, et al., Modeling and optimization of process parameters of biofilm reactor for wastewater treatment, Sci. Total Environ. 787 (2021) 147624, https://doi.org/10.1016/j.scitotenv.2021.147624.
[171] M. Irfan, et al., Response surface methodology and artificial neural network modelling of membrane rotating biological contactors for wastewater treatment, Materials 15 (2022), https://doi.org/10.3390/ma15051932.
[172] K.M. Desai, et al., Comparison of artificial neural network (ANN) and response surface methodology (RSM) in fermentation media optimization: case study of fermentative production of scleroglucan, Biochem. Eng. J. 41 (2008) 266−273, https://doi.org/10.1016/j.bej.2008.05.009.
[173] F. Mohammadi, et al., Modeling and sensitivity analysis of the alkylphenols removal via moving bed biofilm reactor using artificial neural networks: comparison of levenberg marquardt and particle swarm optimization training algorithms, Biochem. Eng. J. 161 (2020) 107685, https://doi.org/10.1016/j.bej.2020.107685.
[174] S. Shi, G. Xu, Novel performance prediction model of a biofilm system treating domestic wastewater based on stacked denoising auto-encoders deep learning network, Chem. Eng. J. 347 (2018) 280−290, https://doi.org/10.1016/j.cej.2018.04.087.
[175] A. Qamar, et al., A deep neural networks framework for in-situ biofilm thickness detection and hydrodynamics tracing for filtration systems, Sep. Purif. Technol. 301 (2022) 121959, https://doi.org/10.1016/j.seppur.2022.121959.
[176] A. Sinharoy, K. Pakshirajan, Methane free biohydrogen production from carbon monoxide using a continuously operated moving bed biofilm reactor, Int. J. Hydrogen Energy 46 (2021) 306−313, https://doi.org/10.1016/j.ijhydene.2020.09.250.